Theoretical Study of the Light-Induced Spin Crossover Mechanism in $[Fe(mtz)_6]^{2+}$ and $[Fe(phen)_3]^{2+}$

Carmen Sousa,[*,†] Coen de Graaf,[‡,¶,§] Andrii Rudavskyi,[§] and Ria Broer[§]

Departament de Ciència de Materials i Química Física and Institut de Química Teòrica i Computacional, Universitat de Barcelona, C/ Martí i Franquès 1, 08028 Barcelona, Catalunya, Spain, ICREA, Pg. Lluís Companys 23, 08010 Barcelona, Catalunya, Spain, Departament de Química Física i Inorgànica, Universitat Rovira i Virgili, Marcel·lí Domingo s/n, 43007 Tarragona, Catalunya, Spain, and Zernike Institute for Advanced Materials, University of Groningen, Nijenborgh 4, 9747 AG Groningen, The Netherlands

E-mail: c.sousa@ub.edu

[*]To whom correspondence should be addressed
[†]Universitat de Barcelona
[‡]ICREA
[¶]Universitat Rovira i Virgili
[§]University of Groningen

Abstract

The deactivation pathway of the light induced spin crossover process in two Fe(II) complexes has been studied by combining Density Functional Theory calculations for the geometries and the normal vibrational modes and highly correlated wave function methods for the energies and spin-orbit coupling effects. For the two systems considered, the mechanism of the photoinduced conversion from the low-spin singlet to the high-spin quintet state implies two intersystem crossings through intermediate triplet states. However, while for the $[Fe(mtz)_6]^{2+}$ complex, the process occurs within few picoseconds and involves uniquely metal-centered electronic states, for the $[Fe(phen)_3]^{2+}$ system the deactivation channel involves both metal to ligand charge transfer and metal-centered states and takes place in a femtosecond time scale.

November 30, 2017

Introduction

The interest in molecular based materials with photo-switchable properties has increased in the last years due to their potencial use in technological applications, such as sensors or optical memory devices.[1–4] Among these materials, spin crossover (SCO) systems based on transition metal molecular complexes have been extensively studied since their properties can be optically switched in a extremely short time scale.[5] In fact, at low temperatures the spin state of the metal can be changed from a low-spin (LS) ground state to a high-spin (HS) metastable state by light irradiation. This phenomenon is known as Light-Induced Excited Spin State Trapping (LIESST)[6] and was initially found in Fe(II) complexes[6–10] and later observed in systems containing Fe(III)[11–14] and Ni(II).[15–17] A broad range of Fe(II)-based materials have been investigated both in solution and in the solid state, where cooperative effects are of interest. Particularly, six-coordinated iron(II) complexes with nitrogen-donor ligands in a nearly octahedral geometry have been the subject of intense research since these systems provide the largest structural changes under spin conversion and, therefore, favor

cooperative transitions in the solid state. As a matter of fact, the spin crossover process in Fe(II)-N_6 complexes from the LS ($^1A_1$) ground state to the HS ($^5T_2$) state is accompanied by an enlargement of the Fe-N distance of around 0.2 Å due to the occupation of the antibonding e orbitals in the quintet HS state.[18] The study of the light-induced spin crossover process in Fe(II) complexes from the singlet LS ground state to the quintet HS state has received much attention. The mechanism of the process has been qualitatively described by Hauser.[6] After irradiation of the system into the LS absorption bands at low temperatures, the HS state is populated through a double intersystem crossing involving intermediate triplet states. In this photocycle, electronic states of different nature may be involved. Those include states centered on the metal (metal-centered, MC), centered on the ligand (ligand-centered, LF) or states that involve excitations from one to the other or viceversa, i.e., metal to ligand charge transfer (MLCT) or ligand to metal charge transfer (LMCT) states. Hence, the photophysics of the spin conversion is an intricate problem that results from the interplay of several factors: electronic states of different character play a role, important structural changes go along the conversion and various non-radiative processes are involved, such as internal conversion (IC), that is, transitions between electronic states of the same spin; intersystem crossing (ISC), which involves electronic states of different spin multiplicities; and intramolecular vibrational redistribution (IVR), where the vibrational energy is redistributed between different vibrational modes. For these reasons, together with the extremely short time scale of the spin conversion, a detailed interpretation of the photophysics of the process has not been possible until recently. The development of ultrafast spectroscopic techniques in the last fifteen years opened the possibility to explore phenomena on the time scale of molecular vibrations.[5,19] Progress on optical and X-ray techniques, as pump-probe Transient Absorption Spectroscopy,[20,21] Ultrafast X-ray Absorption and Emission spectroscopies[22–24] and Ultrafast Fluorescence,[25] has been crucial to get insight into the mechanisms of photophysical and photochemical processes in transition metal complexes with resolution in the femtosecond scale. Although the experimental information acquired by these techniques is of

key importance, the in depth understanding of these processes is only possible in combination with state-of-the-art computational methodologies.

A paradigmatic system that has been extensively studied, both experimentally and by means of computational approaches, is the iron(II)tris(bipyridine) complex in aqueous solution, $[Fe(bpy)_3]^{2+}$. It is observed that by irradiating with visible light, the system is excited to the ^{1}MLCT state and afterwards, it decays into the HS MC $^5T_2$ state in a femtosecond time scale with almost unity quantum yield. A large number of studies have been performed in order to ascertain the steps of the mechanism and the timescale of the photoinduced SCO process. From these studies, different interpretations have been proposed. Some authors claim that a first step involves singlet to triplet conversion within the MLCT manifold and subsequently a direct deactivation from the ^{3}MLCT to the $^5T_2$ state takes place.[19,21,24,26,27] Alternatively, mechanisms involving either intermediate Fe centered triplet states[25,28–30] or ^{5}MLCT states[31] have also been suggested.

In this work, we study the light induced spin crossover process in two Fe(II) systems by means of *ab initio* computational methods. The computational approach is based on a combination of Density Functional Theory (DFT) calculations for the geometries and vibrational frequencies of the relevant electronic states, with multiconfigurational wave function calculations that allow us to compute accurate electronic energies and spin-orbit coupling matrix elements of the spin states involved.[28,29,32,33] From these data, intersystem-crossing rate constants can be derived from a time-dependent approach based on Fermi's golden rule.[34]

Two different Fe(II)-N_6 isolated complexes have been studied (Figure 1). First, the $[Fe(mtz)_6]^{2+}$ complex, where mtz refers to the 1-methyl-tetrazole monodentate ligand. In fact, this system is a model compound of the $[Fe(ptz)_6]^{2+}$ complex, with ptz=1-propyl-tetrazole, that has been shown to undergo light induced spin crossover both in neat solid state compounds, like $Fe(ptz)_6(BF_4)_2$,[10] and in diluted systems, as $Zn_{1-x}Fe_x(ptz)_6(BF_4)_2$.[35] From these studies, it was concluded that after excitation into the absorption bands of the

singlet LS state, the quintet HS state is populated via two intersystem crossings involving the intermediate MC $^3T_1$ state. The intersystem crossing rate constants were estimated to be in the range 10^{10}- 10^{12} s^{-1} with a branching ratio from the $^3T_1$ state to the $^1A_1$ ground state and $^5T_2$ state of approximately 1:4. Recently, the intermediate states of the LIESST and reverse-LIESST pathways in the $Fe(ptz)_6(BF_4)_2$ SCO compound have been elucidated. In both processes, triplet states centered on the iron are involved. In particular, the lifetime of the $^3T_2$ intermediate state of the LIESST process was estimated to be of 1.2 ps, while the $^3T_1$ plays a role in the reverse-LIESST with a decay time of 39 ps.[36]

The second material studied is a bidentate Fe(II) system, the $[Fe(phen)_3]^{2+}$ complex, with phen=1,10-phenanthroline (see Figure 1). The photoinduced spin conversion of this system in solution has been studied by transient absorption spectroscopy.[37] After initial excitation of the system to the singlet MLCT band, the experimental data suggest a very fast transition to the triplet MLCT band, within less than 100 fs, and subsequently the system decays into a vibrationally excited quintet HS state in about 220 fs. Vibrational cooling within the $^5T_2$ state is estimated to be around 8.6 ps and the final HS to LS relaxation is completed in $\sim$ 1 ns (800 ps in water solution and 1.1 ns in acetonitrile). Hence, these authors suggested the following relaxation scheme: ^{1}MLCT $\rightarrow$ ^{3}MLCT $\rightarrow$ $^5T_2{}^*$ $\rightarrow$ $^5T_2$, where $^5T_2{}^*$ refers to a vibrational excited state. The same mechanism has been proposed in an analogous study of a similar system, the $[Fe(2\ CH_3 - phen)_3]^{2+}$ complex.[38]

Here, the photocycle of the LS to HS conversion for these two complexes will be studied. It will be shown that the deactivation channel of the $[Fe(phen)_3]^{2+}$ complex involves both MLCT and MC states and takes place in a femtosecond time scale, while the light induced SCO in the $[Fe(mtz)_6]^{2+}$ system occurs within few picoseconds and involves exclusively MC electronic states.

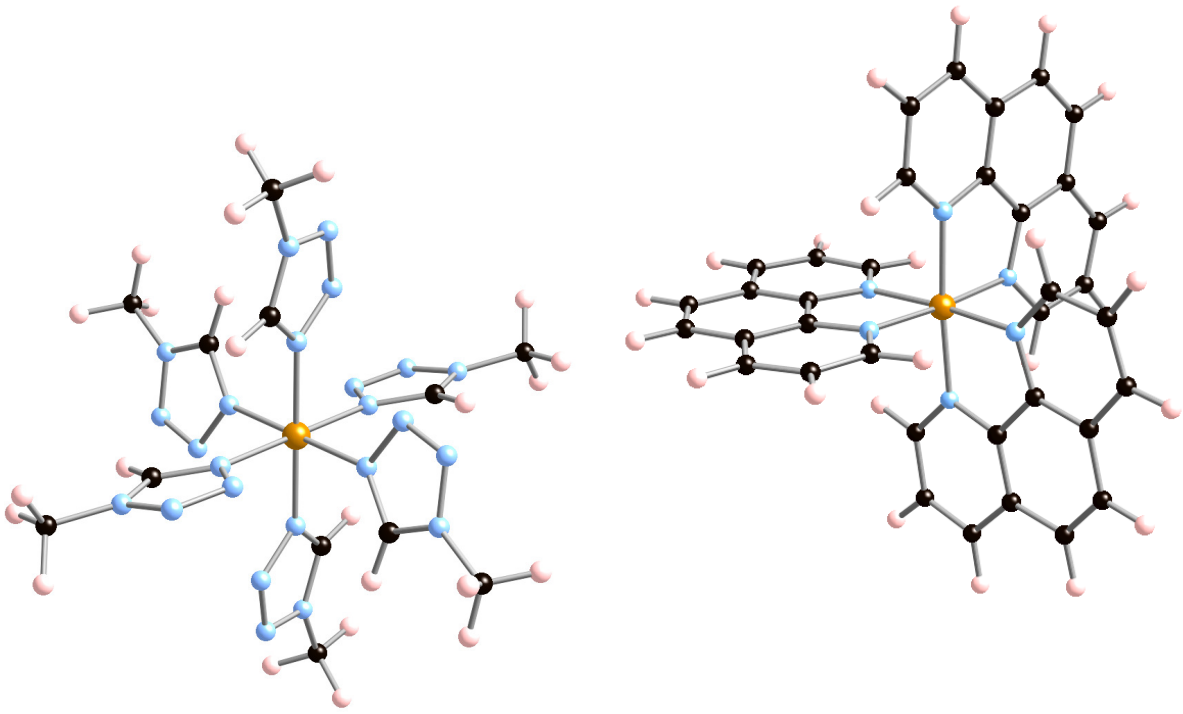

$\mathbf{[Fe(mtz)_6]^{2+}}$ $\mathbf{[Fe(phen)_3]^{2+}}$

Figure 1: Molecular complexes investigated in this study. Fe is in the center of the complexes, represented by a light brown sphere, black spheres represent C, blue is N and pink is H.

Methodology

The accurate theoretical description of the light induced SCO process requires the computation of several components. On one hand, optimized equilibrium geometries and vibrational frequencies for all the electronic states involved in the photocycle are needed. On the other hand, potential energy curves along the reaction coordinate that connects the LS with the HS state give insight in the deactivation mechanism. In addition, energy differences between the various electronic states and spin-orbit coupling matrix elements are needed to estimate the intersystem crossing rate constants between electronic states of different spin multiplicity. In order to achieve this goal, a combined computational approach using both DFT and wave function based methods has been proposed. This procedure has been successfully applied in a previous study of the deactivation process in the $[Fe(bpy)_3]^{2+}$ complex[29] and the Fe(III) complex $[Fe(qsal)_2]^+$, with Hqsal = 2-[(8-quinolinylimino)methyl]phenol.[39]

Optimized geometries and vibrational frequencies have been computed within the DFT framework using the Perdew-Becke-Ernzerhof (PBE0) hybrid functional[40] and a triple zeta valence plus polarization basis set,[41] as implemented in the TurboMole 6.3 package.[42,43] The geometry optimizations of the lowest singlet, triplet and quintet states were performed using the standard unrestricted DFT formalism and the vibrational frequencies were computed analytically within the harmonic approximation. Instead, the geometries of the excited states have been determined by Time Dependent DFT (TD-DFT)[44,45] calculations and the harmonic frequencies computed numerically. No symmetry restrictions were imposed in the DFT calculations.

The energies of the different spin states have been computed by means of a multiconfigurational wave function based method, the CASSCF/CASPT2 approach. One-dimensional CASPT2 potential energy curves along the reaction coordinate, defined as a linear interpolation between the HS and LS PBE0 optimized structures, have been computed. The effects of spin-orbit coupling on the relative energies between the different electronic states are only minor and have not been included. This approach has proved to accurately describe

thermal and optical SCO processes in several materials.[28,30,32,46–49] The CASSCF/CASPT2 method[50] is a two step approach in which a second-order perturbation treatment is applied on a complete active space self-consistent field (CASSCF) reference wave function. This methodology is implemented in the MOLCAS 7.4 software.[51,52] Atomic natural orbital basis sets, specifically derived to allow for relativistic effects, have been used[53,54] with the following contraction scheme: (7s, 6p, 5d, 4f, 3g, 2h) for Fe, (4s, 3p, 1d) for the N atoms bonded to the Fe, (3s, 2p) for the remainding N and C atoms and (2s) for H. The active space used to construct the CASSCF wave functions contains ten electrons distributed among 15 orbitals, the five 3d Fe orbitals, two e-like σ-bonding ligand orbitals, three ligand virtual orbitals of π^* character and a second set of diffuse Fe-3d orbitals to account for the large electron correlation effects in the 3d-shell. This active space assures a proper and balanced description of the different MC and MLCT states.[32,46,55] CASPT2 accounts for the remaining electron correlation by correlating all the electrons except the deep core electrons ($1s^2$ for N and C and $1s^2$, $2s^2$, $2p^6$ for Fe). In the second order perturbative CASPT2 method, the standard zeroth-order Hamiltonian has been used.[56] Scalar relativistic effects were included using a Douglas-Kroll-Hess Hamiltonian[57,58] while the spin-orbit coupling matrix elements between the various electronic states were computed by the spin-orbit state interaction approach using the CASSCF wave functions .[59,60] For the $[Fe(mtz)_6]^{2+}$ and $[Fe(phen)_3]^{2+}$ systems studied here, the CASSCF/CASPT2 calculations were performed within the C_i and C_2 symmetry point groups, respectively. However, since the local geometry around the central atom is quasi octahedral, the electronic states were labeled according to the O symmetry group.

Intersystem crossing rate constants, k_{ISC}, have been determined applying a procedure based on the Fermi's golden rule and a time-dependent approach as implemented in the VIBES program.[34,61] This methodology has been successfully applied to different kind of systems.[29,62–64] Within this approximation, ISC rate constants can be calculated as:

$$k_{ISC} = |\langle \Phi_I | \hat{\mathcal{H}}_{SO} | \Phi_F \rangle|^2 \int_{-\infty}^{\infty} dt G(t) e^{it(\Delta E_{IF} + \frac{1}{2} Tr\Omega_I)} \quad (1)$$

where Φ_I and Φ_F refer to the initial and final electronic states, ΔE_{IF} the energy difference between both states, $\hat{\mathcal{H}}^{SO}$ is the spin-orbit coupling operator, $G(t)$ is a time-dependent correlation function that contains information about the vibrational frequencies and normal coordinates, and Ω_I is a diagonal matrix formed by the vibrational frequencies of the initial state. The explicit formula of G(t) is rather lengthy and the interested reader is referred to Ref.[34] for more detailed information. Here, we only remark that G(t) contains, apart from the diagonal matrices Ω_I and Ω_F, also the Duschinsky matrix $\mathbf{J}$ and the translation vector $\mathbf{D}$ that are used to express the normal coordinates of the final state $\mathbf{Q_F}$ in those of the initial state $\mathbf{Q_I}$ by the so-called Duschinsky transformation $\mathbf{Q_F} = \mathbf{J}\mathbf{Q_I} + \mathbf{D}$. The combination of energy difference between initial and final state, the size of the off-diagonal matrix elements of $\mathbf{J}$, and the norm of the translation vector $\mathbf{D}$ determines how large the final vibrational overlap between the different electronic states will be. Here, the relative energies of the different electronic states, ΔE_{IF}, and the spin-orbit coupling matrix elements have been computed within the CASSCF/CASPT2 approach. Vibrational frequencies and normal coordinates within the harmonic approach have been obtained from PBE0 DFT calculations.

Results and Discussion

Light induced SCO in the $[Fe(mtz)_6]^{2+}$ complex

The geometries of the $^1A_1$ ground state and the metastable $^5T_2$ HS state of the $[Fe(mtz)_6]^{2+}$ complex have been computed by means of DFT calculations in previous works.[33,49] It was shown that while interatomic distances, and particularly, Fe-N distances, were in accordance with experiment, all DFT functionals considered lead to unphysical rotation angles of the methyl-tetrazole ligands, $\sim 45°$, to minimize steric effects. This results from the lack of environment effects of the rest of the crystal that counterbalance the steric repulsion. Taking into account such effects through an embedded two center complex, the rotation angles are

well reproduced, with an average angle for the active site around 12°. In order to take into account this geometrical parameter, the CASPT2 potential energy curves of all the relevant electronic states have been computed along a reaction coordinate corresponding to the symmetric stretching mode of the Fe-N_6 coordination sphere fixing the rotation angle of the ligands at 10°. At each scan of the reaction coordinate, the geometry of the ligands has been optimized by PBE0 and the energy computed by CASPT2. The computed vertical excitation energies for the lowest transitions from the LS and HS states are collected in Table 1. These excitations involve electronic states centered in the Fe(II) atom, other excitations involving MLCT or LMCT states lie at higher energies for this particular system. As can be seen from Table 1, the $[Fe(mtz)_6]^{2+}$ complex accurately reproduces the experimental data corresponding to the $Fe(ptz)_6(BF_4)_2$ system, meaning that the different substituents (methyl or propyl) of the tetrazole rings have a negligible effect on the optical transitions centered on the metal. Particularly, the first step in the LIESST process, the excitation from the $^1A_1$ ground state to the first excited singlet, $^1T_1$, is well reproduced.

Table 1: Vertical CASPT2 excitation energies (in cm^{-1}) for the $[Fe(mtz)_6]^{2+}$ complex and experimental data for $Fe(ptz)_6(BF_4)_2$.[10]

Transition	CASPT2	Experiment
$^1A_1 \rightarrow {}^1T_1$	17509	18200
$^1A_1 \rightarrow {}^3T_1$	9646	10280
$^1A_1 \rightarrow {}^3T_2$	14361	14330
$^5T_2 \rightarrow {}^5E$	12682	11760

The CASPT2 one-dimensional potential energy curves for the lowest singlet, triplet and quintet states are plotted in Figure 2. Since all these electronic states arise from the different distributions of the $3d^6$ electrons in the Fe(II) atom, the standard active space of 10 electrons in twelve orbitals[55] suffices and there is no need to add extra occupied or virtual ligand orbitals. As can be seen in Figure 2, the Fe-N equilibrium distance for the LS state is 1.95 Å and the corresponding value for the HS state is 0.2 Å larger, as expected in Fe(II)-N_6 complexes. The excited singlet, $^1T_1$, and the intermediate triplet states, $^3T_2$ and $^3T_1$, show

a minimum at an intermediate Fe-N distance, around 2.05 Å , due to the occupation of an antibonding e orbital in a ($t_2^5e^1$) configuration. The Jablonski diagram of the electronic states involved in the spin conversion (Figure 2) shows that after light irradiation, the excited $^1T_1$ state is populated. This state crosses with the final HS $^5T_2$ in the Franck-Condon region, and the intermediate triplet states also interact with the HS state. To quantify these interactions, inclusion of spin-orbit coupling is necessary. In Table 2 the square of the spin-orbit coupling matrix elements for the possible interactions are presented. These elements have been computed at the geometry corresponding to the LS state, i.e. in the Franck-Condon region. Nevertheless, it has been demonstrated that spin-orbit coupling does not significantly change with the Fe-ligand distance, especially when MC states are involved.[32] As can be seen in Table 2, all the values of the SO term are of similar order of magnitude (between 10^4 - 10^5 cm^{-2}) except for the $^3T_2 \rightarrow {}^1A_1$ transition. The spin-orbit coupling matrix element between these two states is strictly zero in the O_h point group by symmetry reasons. Here, due to the nearly-octahedral symmetry of the compound, this term is not zero but of small value, $\sim 10^2$ cm^{-2}. Regarding the SO term, the $^1T_1$ state populated after absorption, shows important interactions with the lowest $^3T_2$ and $^3T_1$ intermediate states while there is no direct SO coupling between the singlet $^1T_1$ and the quintet $^5T_2$ state. In order to understand the photocycle and to quantify the timescale of the process, apart from the spin-orbit coupling term, the vibrational contribution as defined in Eq. 1 is needed. The results of this term along with the ISC rate constants are presented in Table 2. Inclusion of the vibrational contribution reveals that from the photoexcited $^1T_1$ state the system can cross to the $^3T_2$ state in 36 ps, while deactivation to the lower-lying $^3T_1$ state is not favored because the vibrational contribution is four orders of magnitude smaller. Since the geometrical structure of the two triplet states is very similar, the large difference in the vibrational term is explained by the larger energy difference between the $^1T_1$ and $^3T_1$ states. From the $^3T_2$ state, the complex could eventually decay either into the initial LS or into the HS, thus completing the spin conversion. Our results show that the decay to the

$^5T_2$ HS is preferred since the ISC rate constant is two orders of magnitude larger than the corresponding deactivation to the initial LS state. Based on these results, the photoinduced spin conversion can be explained as follows: after populating the $^1T_1$ by light irradiation, the $^3T_2$ state is reached in 36 ps, and throughout a second ISC the $^5T_2$ is populated within 12 ps. According to this interpretation, the whole process takes place within 50 ps with a high quantum efficiency and involves two ISC, $^1T_1 \rightarrow {}^3T_2 \rightarrow {}^5T_2$. These results are in agreement with previous experimental studies indicating that the process takes place in few picoseconds[10] and with a recent study that pointed to the $^3T_2$ state as intermediate state in the LIESST process.[36]

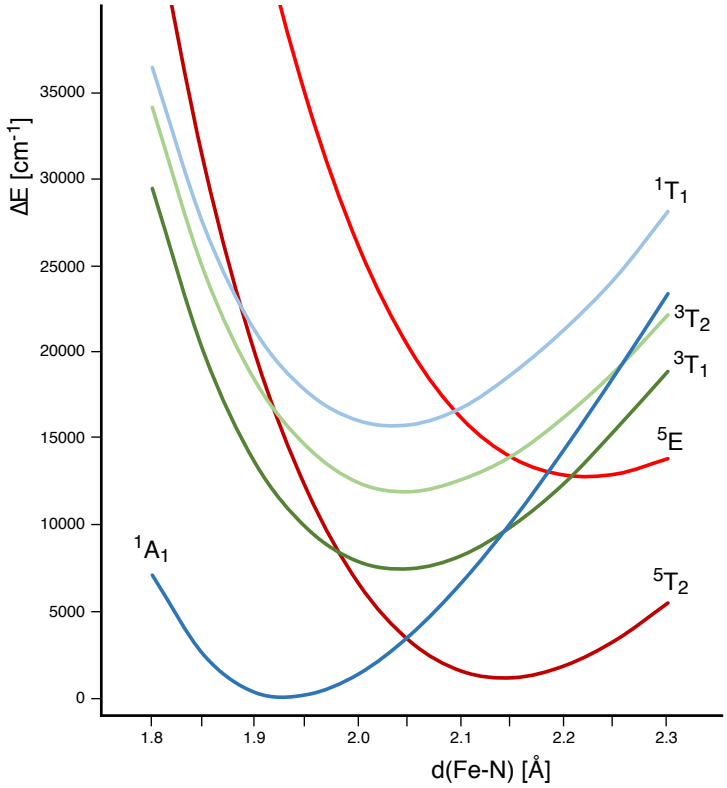

Figure 2: CASPT2 potential energy curves of the lowest electronic states of $[Fe(mtz)_6]^{2+}$ as function of the Fe-N distance.

Examining the results in Table 2, it should be noticed that the highest ISC rate constants correspond to the deactivation from the lowest triplet state, $^3T_1$, to the LS and HS states. Both processes occur in the range of hundred femtoseconds. This fast channel can only be

of importance if after excitation to the $^1T_1$ state, the $^3T_1$ state is populated. However, as previously commented, the direct $^1T_1 \rightarrow {}^3T_1$ transition is not favored. An alternative path involving internal conversion from the $^3T_2$ to the $^3T_1$ state opens this possibility. Unfortunately, the time scale of the internal conversion within the two triplet states cannot be estimated, but previous studies gave evidence that this process is expected to be fast.[29] Under this assumption, a possible deactivation path involving two ISC and a IC is as follows: $^1T_1 \rightarrow {}^3T_2 \rightarrow {}^3T_1 \rightarrow {}^5T_2$. This mechanism takes place in picoseconds, as experimentally measured, however it leads to a branching ratio that favors the LS ground state, with a value of 2:1 for the $^3T_1 \rightarrow {}^1A_1$ and $^3T_1 \rightarrow {}^5T_2$ conversions. This is contrary to the observed quantum efficiency that favors the HS state and therefore, this fact plays against this proposal. On the other hand, the possibility that the two mechanisms commented here take place simultaneously cannot be ruled out.

Table 2: Intersystem crossing rates between the relevant electronic states of $[Fe(mtz)_6]^{2+}$. The spin-orbit and vibrational contributions (cf. Eq. 1) are separately given. t denotes the deactivation time.

Φ_I	Φ_F	SO term (cm^{-2})	vib. term (cm^2s^{-1})	k_{ISC} (s^{-1})	t
$^1T_1$	$^3T_2$	$1.2 \cdot 10^5$	$2.3 \cdot 10^5$	$2.8 \cdot 10^{10}$	36 ps
$^3T_2$	$^1A_1$	$5.3 \cdot 10^2$	$1.6 \cdot 10^6$	$8.5 \cdot 10^8$	1.2 ns
$^3T_2$	$^5T_2$	$9.8 \cdot 10^4$	$9.4 \cdot 10^5$	$8.2 \cdot 10^{10}$	12 ps
$^1T_1$	$^3T_1$	$1.6 \cdot 10^4$	$5.3 \cdot 10^1$	$8.5 \cdot 10^5$	$>$ 100 ns
$^3T_1$	$^1A_1$	$9.8 \cdot 10^4$	$1.0 \cdot 10^8$	$9.8 \cdot 10^{12}$	102 fs
$^3T_1$	$^5T_2$	$2.4 \cdot 10^5$	$2.1 \cdot 10^7$	$5.0 \cdot 10^{12}$	200 fs

Light induced SCO in the $[Fe(phen)_3]^{2+}$ complex

As a first step, a full geometry optimization of the ground state of the $[Fe(phen)_3]^{2+}$ complex in vacuo has been performed by means of DFT PBE0 calculations. The resulting optimized geometry possesses D_3 symmetry with all Fe-N distances equal to 2.003 Å , which is in good agreement with the experimental average value of 1.983 Å.[65] The optimized structures for the rest of the electronic states involved in the light induced spin conversion have been determined

either by standard DFT calculations (lowest triplet and quintet states, $^3T_1$ and $^5T_2$) or by the TD-DFT methodology (singlet excited states, $^1T_1$ and ^1MLCT). Only the lowest state of a given nearly degenerated manifold of states has been computed. It is assumed that the other states of the manifold have the same geometry and vibrational frequencies. For the $^3T_1$ and $^5T_2$ the optimized geometries slightly deviate from the D_3 point group. Average PBE0 optimized Fe-N distances for the $^1T_1$ and $^3T_1$ states are 2.101 Å and 2.109 Å respectively, while for the quintet $^5T_2$ state it is 2.206 Å . As in the previous Fe(II) system, the Fe-N distance increases regularly ∼0.1 Å when one electron is promoted from the non-bonding t_2 orbitals to an antibonding e orbital. It is important to notice that the average optimized Fe-N distance for the ^1MLCT state is 1.987 Å , that is, very close to the Fe-N distance in the $^1A_1$ ground state, in line with the fact that no antibonding e-like orbital is occupied in the lower ^1MLCT states. In order to obtain the optimal geometric parameters at the CASPT2 level of calculation, a hybrid DFT/CASPT2 approach as described before, has been applied. A scan of the Fe-N distance around the equilibrium distance has been performed and at each point the geometry of the ligands were optimized by PBE0 calculations. In this way, the CASPT2 optimized Fe-N distance for the ground state turns out to be 1.92 Å , which is somewhat shorter that the value corresponding to a full PBE0 optimization. Equivalently, the Fe-N distances corresponding to the CASPT2 minimum for the $^5T_2$ and $^3T_1$ are 2.15 and 2.04 Å , respectively.

The vertical absorption spectrum from the $^1A_1$ ground state has been computed by means of CASPT2 calculations. At the LS geometry, the lowest excited singlet state is a MC state lying about 2.4 eV above the $^1A_1$. However, for the $[Fe(phen)_3]^{2+}$ complex, and at difference of the $[Fe(mtz)_6]^{2+}$ system, the singlet MLCT states lie in the same energy region as the lowest singlet MC ligand field states. Indeed, the lowest ^1MLCT states span in the energy range of 2.5-3.0 eV. This is slightly higher, but very close, to the peak measured in the absorption spectrum of $[Fe(phen)_3]^{2+}$ in acetonitrile, at approximately 2.5 eV.[66] The ^3MLCT states form a band in the same energy region as the ^1MLCT states and with the

same Fe-N equilibrium distance. The ^5MLCT states, instead, appear at much higher energies and spread over 3.8-4.6 eV above the LS state and, therefore, these states are not involved in the LIESST process. Finally, the lowest triplet Fe centered state, $^3T_1$, appears at 1.4 eV above the $^1A_1$ state, however a singlet-triplet transition is not allowed by the dipole selection rule. Hence, the first state populated in the $[Fe(phen)_3]^{2+}$ complex by light irradiation is the ^1MLCT state, as found in a similar bidentate ligand complex, the $[Fe(bpy)_3]^{2+}$ system. This $^1A_1$ to singlet ^1MLCT excitation carries intensity since it is symmetry allowed in a perfect octahedral geometry, while the ligand field $^1A_1$ to $^1T_1$ transition is symmetry forbidden and only displays a weak signal in the absorption spectrum.

In order to elucidate the relaxation mechanism, all states that can be involved in the process have to be taken into account to analyze all the possible deactivation paths. Spin-orbit coupling matrix elements involving all low-lying electronic states have been calculated. These include the sixteen lowest singlet, triplet and quintet states, which leads to 144 spin states and the corresponding 144x144 spin-orbit matrix. The results of the spin-orbit contribution, together with the vibrational term and the rate constant for the intersystem crossings between the relevant electronic states, are reported in Table 3. Deactivation times are also detailed when pertinent. In light of our results, after population of the ^1MLCT state by irradiation, the system most probably deactivates to the ^3MLCT manifold. As can be seen in Table 3, this process is favored both by a large spin orbit coupling term and by vibrational terms, resulting in a large rate constant, $2.8{\cdot}10^{13}$ s^{-1}, and a deactivation time of 36 fs. This result is in agreement with transient absorption spectroscopy measures of $[Fe(phen)_3]^{2+}$ in solution, that estimated the relaxation time towards the ^3MLCT state in less that 100 fs.[37] Other deactivation routes from the ^1MLCT to triplet MC states are two orders of magnitude slower, and therefore, less optimal. Once the ^3MLCT state is reached, this state can directly relax to either the $^1A_1$ LS ground state or the $^5T_2$ HS state. Relaxation back to the LS state is very slow, since the two contributions, vibrational and spin-orbit, are small. Alternatively, direct deactivation to the $^5T_2$ is favored by a large vibrational term, however the small spin-

orbit coupling between ^3MLCT - $^5T_2$, 2.7·10^3 cm^{-2}, hinders this path. This small direct SO coupling can be justified by the fact that the orbital occupation of the two electronic states differs by a double electron transfer, from a $t_2^5e^0L^1$ configuration of the ^3MLCT to a $t_2^4e^2$ configuration in the $^5T_2$. Nevertheless, on the basis of the present calculations, we cannot exclude the possibility that indirect spin-orbit terms, that is, SO mediated by other spin electronic states, could be of importance and make this channel viable. A different path to explain the relaxation from the ^3MLCT state to the HS state can involve the Fe-centered $^3T_1$ state. The results in Table 3 show that the deactivation from the $^3T_1$ to the $^5T_2$ state is very effective and takes place in around 100 fs, while relaxation back to the $^1A_1$ is two orders of magnitude slower. A fast population of the $^3T_1$ state is only possible by internal conversion from the ^3MLCT states, since the other possibilities, either from the ^1MLCT or the $^1T_1$ states, exhibit deactivation times one order of magnitude larger than the measured ones. As a consequence, a plausible deactivation path could involve both MLCT and MC states as follows: $^1MLCT \rightarrow {}^3MLCT \rightarrow {}^3T_1 \rightarrow {}^5T_2$, in which the first intersystem crossing implying singlet and triplet MLCT states takes place in 36 fs and the second ISC involving iron centered states, $^3T_1$ and $^5T_2$, occurs in 102 fs. As commented before, we have not estimated the timescale of the internal conversion between the ^3MLCT and $^3T_1$ states, but this spin allowed transition is expected to be very fast. In summary, the timescale of the deactivation process based on our results is in overall accord with the experimental observation that the process takes place in around 300 fs via ^3MLCT states.

Summary and Conclusions

The mechanism of the photoinduced spin crossover process in two Fe(II) complexes has been studied by means of a combination of theoretical methods. Density functional theory calculations allow to compute optimized geometries and vibrational spectra, multiconfigurational CASSCF and CASPT2 calculations give sufficiently accurate energies, spin-orbit coupling

Table 3: Intersystem crossing rates between the relevant electronic states of $[Fe(phen)_3]^{2+}$. The spin-orbit and vibrational contributions (cf. Eq. 1) are separately given. t denotes the deactivation time.

Φ_I	Φ_F	SO term (cm^{-2})	vib. term (cm^2s^{-1})	k_{ISC} (s^{-1})	t
^1MLCT	^3MLCT	$1.1{\cdot}10^5$	$2.6{\cdot}10^8$	$2.8{\cdot}10^{13}$	36 fs
^1MLCT	$^3T_2$	$1.3{\cdot}10^4$	$8.3{\cdot}10^4$	$1.1{\cdot}10^9$	–
^1MLCT	$^3T_1$	$1.4{\cdot}10^4$	$6.0{\cdot}10^7$	$8.1{\cdot}10^{11}$	>1 ps
^3MLCT	$^1A_1$	$2.5{\cdot}10^3$	$4.7{\cdot}10^4$	$2.6{\cdot}10^8$	–
^3MLCT	$^5T_2$	$2.7{\cdot}10^3$	$5.0{\cdot}10^7$	$1.4{\cdot}10^{11}$	>1 ps
$^1T_1$	$^3T_2$	$2.8{\cdot}10^5$	$4.6{\cdot}10^3$	$1.3{\cdot}10^9$	–
$^3T_2$	$^1A_1$	$2.0{\cdot}10^4$	$6.0{\cdot}10^0$	$1.2{\cdot}10^5$	–
$^3T_2$	$^5T_2$	$7.7{\cdot}10^5$	$6.3{\cdot}10^2$	$4.9{\cdot}10^8$	–
$^1T_1$	$^3T_1$	$1.7{\cdot}10^4$	$2.6{\cdot}10^7$	$4.5{\cdot}10^{11}$	>1 ps
$^3T_1$	$^1A_1$	$8.2{\cdot}10^5$	$5.7{\cdot}10^4$	$4.7{\cdot}10^{10}$	–
$^3T_1$	$^5T_2$	$1.9{\cdot}10^6$	$5.1{\cdot}10^6$	$9.8{\cdot}10^{12}$	102 fs

matrix elements and relative energies, and intersystem crossing transition rate constants are derived by a time-dependent approach based on Fermi's golden rule. This integrated strategy permits to describe the essential features of the light induced spin conversion and helps to elucidate the mechanism of the process, in conjunction with the experimental information available. Specifically, the electronic states involved in the process can be assessed and the rates of the intersystem crossings quantified.

In this work, this methodology has been applied to two Fe(II) complexes, $[Fe(mtz)_6]^{2+}$ and $[Fe(phen)_3]^{2+}$. The light induced spin conversion in the $[Fe(mtz)_6]^{2+}$ complex starts by populating the $^1T_1$ metal centered state by photoirradiation. Metal to ligand charge transfer bands are too high in energy to be accessed. From the $^1T_1$ state, the HS state is reached within 50 ps with a high quantum efficiency following the path $^1T_1 \rightarrow {}^3T_2 \rightarrow {}^5T_2$. This interpretation implies two intersystem crossings between metal centered states and sets the time scale of the process in the order of picoseconds. Both characteristics are in agreement with the experimental data available for the similar $[Fe(ptz)_6]^{2+}$ system.

In the $[Fe(phen)_3]^{2+}$ complex, irradiation of the LS state populates the singlet metal to ligand charge transfer band, ^1MLCT. The ^1MLCT and ^3MLCT states show similar

geometries and lie in the same energy region, therefore a first deactivation step $^1MLCT \rightarrow$ ^3MLCT is favored and occurs within 36 fs. From this state, the process can proceed in two ways: either through an internal conversion to the Fe-centered $^3T_1$ state, that is, $^1MLCT \rightarrow$ $^3MLCT \rightarrow$ $^3T_1 \rightarrow$ $^5T_2$ or by a direct deactivation from the ^3MLCT manifold to the final HS state, $^1MLCT \rightarrow$ $^3MLCT \rightarrow$ $^5T_2$. The first path requires that the internal conversion takes place in the femtosecond time scale and the second route is only possible if second-order spin-orbit coupling is of importance.[67]

The different time scale of the LIESST process in the two complexes derives from the initial step in the deactivation. The ^{1}MLCT-^{3}MLCT intersystem crossing for $[Fe(phen)_3]^{2+}$ is extremely fast, whereas the $^1T_1$-$^3T_2$ crossing in for $[Fe(mtz)_6]^{2+}$ is much slower. The subsequent steps occur on a similar time scale in both complexes.

Acknowledgement

Financial support has been provided by the Spanish Administration (Projects CTQ2014-51938-P and CTQ2015-64618-R), the Generalitat de Catalunya (Projects 2014SGR97, 2014SGR199 and Xarxa d'R+D+I en Química Teòrica i Computacional, XRQTC) and the European Union (COST Action ECOST-Bio CM1305).

References

(1) Kahn, O.; Jay Martinez, C. Spin-transition polymers: from molecular materials toward memory devices. *Science* **1998**, *279*, 44–48.

(2) Hayami, S.; Holmes, S. M.; Halcrow, M. A. Spin-state switches in molecular materials chemistry. *J. Mater. Chem. C* **2015**, *3*, 7775–7778.

(3) Sato, O. Dynamic molecular crystals with switchable physical properties. *Nature Chemistry* **2016**, *8*, 644–656.

(4) Manrique-Juárez, M. D.; Rat, S.; Salmon, L.; Molnár, G.; Quintero, C. M.; Nicu, L.; Shepherd, H. J.; Bousseksou, A. Switchable molecule-based materials for micro- and nanoscale actuating applications: Achievements and prospects. *Coord. Chem. Rev.* **2016**, *308*, 395–408.

(5) Chergui, M. Ultrafast Photophysics of Transition Metal Complexes. *Acc. Chem. Res.* **2015**, *48*, 801–808.

(6) Hauser, A. In *Spin crossover in Transition Metal Compounds II*; Gütlich, P., Goodwin, H. A., Eds.; Top. Curr. Chem.; Springer-Verlag, 2004; Vol. 234; pp 155–198.

(7) McGarvey, J.; Lawthers, I. Photochemically-induced perturbation of the 1A⇌5T equilibrium in FeII complexes by pulsed laser irradiation in the metal-to-ligand charge-transfer absorption band. *J. Chem. Soc. Chem. Commun.* **1982**, *16*, 906.

(8) Decurtins, S.; Gütlich, P.; P., K. C.; Spiering, H.; Hauser, A. Light-Induced excited spin state trapping in a transition metal complex: the hexakis (1-propyltetrazole) iron(II) tetrafluoroborate spin-crossover system. *Chem. Phys. Lett.* **1984**, *105*, 1–4.

(9) Decurtins, S.; Gütlich, P.; P., K. C.; Spiering, H. New examples of light-induced excited spin state trapping (LIESST) in iron(II) spin-crossover systems. *J. Chem. Soc., Chem. Commun.* **1985**, 430–432.

(10) Hauser, A. Intersystem crossing in the $[Fe(ptz)_6](BF_4)_2$ spin crossover system (ptz=1-propyltetrazole). *J. Chem. Phys.* **1991**, *94*, 2741–2748.

(11) Hayami, S.; Gu, Z.-z.; Shiro, M.; Einaga, Y.; Fujishima, A.; Sato, O. First observation of Light-induced excited spin state trapping for an iron(III) complex. *J. Am. Chem. Soc.* **2000**, *122*, 7126–7127.

(12) Juhasz, G.; Hayami, S.; Sato, O.; Maeda, Y. Photo-induce spin transition for iron(III) compounds with π-π interactions. *Chem. Phys. Lett.* **2002**, *364*, 164.

(13) Hayami, S.; Hiki, K.; Kawahara, T.; Maeda, Y.; Urakami, D.; Inoue, K.; Ohama, M.; Kawata, S.; Sato, O. Photo-induced spin transition of iron(III) compounds with π-π intermolecular interactions. *Chem. Eur. J.* **2009**, *15*, 3497.

(14) Clemente-León, M.; Coronado, E.; López-Jordá, M.; Desplanches, C.; Asthana, S.; Wang, H. F.; Létard, J. F. A hybrid magnet with coexistence of ferromagnetism and photoinduced Fe(III) spin-crossover. *Chem. Sci.* **2011**, *2*, 1121.

(15) Thies, S.; Sell, H.; Schütt, C.; Bornholdt, C.; Näther, C.; Tuczek, F.; Herges, R. Light-Induced Spin Change by Photodissociable External Ligands: A New Principle for Magnetic Switching of Molecules. *J. Am. Chem. Soc.* **2011**, *133*, 16243–16250.

(16) Venkataramani, S.; Jana, U.; Dommaschk, M.; Sönnichsen, F. D.; Tuczek, F.; Herges, R. Magnetic Bistability of Molecules in Homogeneous Solution at Room Temperature. *Science* **2011**, *331*, 445.

(17) Ma, H.; Petersen, J. L.; Young Jr., V. G.; Yee, G. T.; Jensen, M. P. Solid-State Spin Crossover of Ni(II) in a Bioinspired N3S2 Ligand Field. *J. Am. Chem. Soc.* **2011**, *133*, 5644.

(18) Guionneau, P.; Marchivie, M.; Bravic, G.; Létard, J.; Chasseau, D. In *Spin crossover in Transition Metal Compounds II*; Gütlich, P., Goodwin, H. A., Eds.; Top. Curr. Chem.; Springer-Verlag, 2004; Vol. 234; pp 97–128.

(19) Cannizzo, A.; Milne, C. J.; Consani, C.; Gawelda, W.; Bressler, C.; van Mourik, F.; Chergui, M. Light-induced spin crossover in Fe(II)-based complexes: The full photocycle unraveled by ultrafast optical and X-ray spectroscopies. *Coord. Chem. Rev.* **2010**, *254*, 2677.

(20) Sun, Q.; Mosquera-Vazquez, S.; LawsonDaku, L.; Gueńeé, L.; Goodwin, H. A.; Vauthey, E.; Hauser, A. Experimental Evidence of Ultrafast Quenching of the ^{3}MLCT Lu-

minescence in Ruthenium(II) Tris-bipyridyl Complexes via a 3dd State. *J. Am. Chem. Soc.* **2013**, *135*, 13660–13663.

(21) Auböck, G.; Chergui, M. Sub-50-fs photoinduced spin crossover in $[Fe(bpy)_3]^{2+}$. *Nature Chemistry* **2015**, *7*, 629–633.

(22) Milne, C. J.; Penfold, T. J.; Chergui, M. Recent experimental and theoretical developments in time-resolved X-ray spectroscopies. *Coord. Chem. Rev.* **2014**, *277-278*, 44–68.

(23) Vankó, G.; Glatzel, P.; Pham, V.; Abela, R.; Grolimund, D.; Borca, C. N.; Johnson, S. L.; Milne, C. J.; Bressler, C. Picosecond Time-Resolved X-Ray Emission Spectroscopy: Ultrafast Spin-State Determination in an Iron Complex. *Angew. Chem. Int. Ed.* **2010**, *49*, 5910.

(24) Bressler, C.; Milne, C.; Pham, V.-T.; ElNahhas, A.; van der Veen, R. M.; Gawelda, W.; Johnson, S.; Beaud, P.; Grolimund, D.; Kaiser, M.; Borca, C. N.; Ingold, G.; Abela, R.; Chergui, M. Femtosecond XANES Study of the Light-Induced Spinc Crossover Dynamics in a Iron(II) Complex. *Science* **2009**, *323*, 489–492.

(25) Zhang, W. et al. Tracking excited-state charge and spin dynamics in iron coordination complexes. *Nature* **2014**, *509*, 345.

(26) Gawelda, W.; Cannizzo, A.; Pham, V.-T.; van Mourik, F.; Bressler, C.; Chergui, M. Ultrafast nonadiabatic dynamics of $[Fe^{II}(bpy)_3]^{2+}$ in solution. *J. Am. Chem. Soc.* **2007**, *129*, 8199–8206.

(27) Consani, C.; Prémont-Schwarz, M.; ElNahhas, A.; Bressler, C.; van Mourik, F.; Cannizzo, A.; Chergui, M. Vibrational Coherences and Relaxation in the High-Spin State of Aqueous $[Fe^{II}(bpy)_3]^{2+}$. *Angew. Chem. Int. Ed.* **2009**, *48*, 1–5.

(28) de Graaf, C.; Sousa, C. Study of the Light-Induced Spin Crossover process of the $[Fe^{II}(bpy)_3]^{2+}$ complex. *Chem. Eur. J.* **2010**, *16*, 4550.

(29) Sousa, C.; de Graaf, C.; Rudavskyi, A.; Broer, R.; Tatchen, J.; Etinski, M.; Marian, C. M. Ultrafast Deactivation Mechanism of the Excited Singlet in the Light-Induced Spin Crossover of [Fe(2,2'-bipyridine)$_3$]$^{2+}$. *Chem. Eur. J.* **2013**, *19*, 17541–17551.

(30) de Graaf, C.; Sousa, C. On the Role of the Metal-to-Ligand Charge Transfer States in the Light-Induced Spin Crossover in Fe^{II}(bpy)$_3$. *Int. J. Quantum Chem.* **2011**, *111*, 3385.

(31) van Veenendaal, M.; Chang, J.; Fedro, A. J. Model of Ultrafast Intersystem Crossing in Photoexcited Transition-Metal Organic Compounds. *Phys. Rev. Lett.* **2010**, *104*, 067401.

(32) Ordejón, B.; de Graaf, C.; Sousa, C. Light-Induced Excited-State Spin trapping in Tetrazole-Based Spin Crossover Systems. *J. Am. Chem. Soc.* **2008**, *130*, 13961–13968.

(33) Rudavskyi, A.; Sousa, C.; de Graaf, C.; Havenith, R. W. A.; Broer, R. Computational approach to the study of thermal spin crossover phenomena. *J. Chem. Phys.* **2014**, *140*, 184318.

(34) Etinski, M.; Tatchen, J.; Marian, C. M. Time-dependent approaches for the calculation of intersystem crossing rates. *J. Chem. Phys.* **2011**, *134*, 154105.

(35) Hauser, A. Intesystem crossing dynamics in Fe(II) coordination compounds. *Coord. Chem. Rev.* **1991**, *111*, 275–290.

(36) Marino, A.; Chakraborty, P.; Servol, M.; Lorenc, M.; Collet, E.; Hauser, A. The Role of Ligand-Field States in the Ultrafast Photophysical Cycle of the Prototypical Iron(II) Spin-Crossover Compound [Fe(ptz)$_6$](BF$_4$)$_2$. *Angew. Chem. Int. Ed.* **2014**, *53*, 3863–3867.

(37) Tribollet, J.; Galle, G.; Jonusauskas, G.; Deldicque, D.; Tondusson, M.; Letard, J.; Freysz, E. Transient absorption spectroscopy of the iron(II) [Fe(phen)$_3$]$^{2+}$ complex:

Study of the non-radiative relaxation of an isolated iron(II) complex. *Chem. Phys. Lett.* **2011**, *513*, 42–47.

(38) Galle, G.; Jonusauskas, G.; Tondusson, M.; Mauriac, C.; Letard, J.; Freysz, E. Transient absorption spectroscopy of the $[Fe(2\ CH3\text{-}phen)_3]^{2+}$ complex: Study of the high spin-low spin relaxation of an isolated iron(II) complex. *Chem. Phys. Lett.* **2013**, *556*, 82–88.

(39) Saureu, S.; de Graaf, C. TD-DFT study of the light-induced spin crossover of Fe(III) complexes. *Phys. Chem. Chem. Phys.* **2016**, *18*, 1233–1244.

(40) Adamo, C.; Barone, V. Toward reliable density functional methods without adjustable parameters: The PBE0 model. *J. Chem. Phys.* **1999**, *110*, 6158.

(41) Weigend, F.; Ahlrichs, R. Balanced basis sets of split valence, triple zeta valence and quadruple zeta valence quality for H to Rn: Design and assessment of accuracy. *Phys. Chem. Chem. Phys.* **2005**, *7*, 3297–3305.

(42) Furche, F.; Ahlrichs, R.; Hättig, C.; Klopper, W.; Sierka, M.; Weigend, F. Turbomole. *WIREs Comput. Mol. Sci.* **2014**, *1*, 91–100.

(43) TURBOMOLE V6.6 2014, a development of University of Karlsruhe and Forschungszentrum Karlsruhe GmbH, 1989-2007, TURBOMOLE GmbH, since 2007; available from http://www.turbomole.com.

(44) Bauernschmitt, R.; Ahlrichs, R. Treatment of electronic excitations within the adiabatic approximation of time dependent density functional theory. *Chem. Phys. Lett.* **1996**, *256*, 454.

(45) Bauernschmitt, R.; Häser, M.; Treutler, O.; Ahlrichs, R. Calculation of excitation energies within time-dependent density functional theory using auxiliary basis set expansions. *Chem. Phys. Lett.* **1997**, *264*, 573.

(46) Suaud, N.; Bonnet, M.-L.; Boilleau, C.; Labèguerie, P.; Guihéry, N. Light-Induced Excited Spin State trapping: Ab Initio Study of the Physics at the Molecular Level. *J. Am. Chem. Soc.* **2009**, *131*, 715–722.

(47) Pierloot, K.; Vancoillie, S. Relative energy of the high-($^5T_{2g}$) and low-($^1A_{1g}$) spin states of the ferrous complexes [Fe(L)(NHS_4)]: CASPT2 versus density functional theory. *J. Chem. Phys.* **2008**, *128*, 034104.

(48) Kepenekian, M.; Le Guennic, B.; Robert, V. Primary Role of the Electrostatic Contributions in a Rational Growth of Hysteresis Loop in Spin-Crossover Fe(II) Complexes. *J. Am. Chem. Soc.* **2009**, *131*, 11498–11502.

(49) Rudavskyi, A.; Havenith, R. W. A.; Broer, R.; de Graaf, C.; Sousa, C. Explanation of the site-specifc spin crossover in $Fe(mtz)_6(BF_4)_2$. *Dalton Trans.* **2013**, *42*, 14702–14709.

(50) Andersson, K.; Malmqvist, P.-Å.; Roos, B. O. Second-Order Perturbation Theory with a Complete Active Space Self-Consistent Field Reference Function. *J. Chem. Phys.* **1992**, *96*, 1218–1226.

(51) Karlström, G.; Lindh, R.; Malmqvist, P.-Å.; Roos, B. O.; Ryde, U.; Veryazov, V.; Widmark, P.-O.; Cossi, M.; Schimmelpfennig, B.; Neogrady, P.; Seijo, L. MOLCAS: a program package for computational chemistry. *Comput. Mater. Sci.* **2003**, *28*, 222–239.

(52) Aquilante, F.; De Vico, L.; Ferré, N.; Ghigo, G.; Malmqvist, P.-Å.; Neogrády, P.; Pedersen, T.; Pitonak, M.; Reiher, M.; Roos, B.; Serrano-Andrés, L.; Urban, M.; Veryazov, V.; Lindh, R. MOLCAS 7: The Next Generation. *J. Comput. Chem.* **2010**, *31*, 224.

(53) Roos, B. O.; Lindh, R.; Malmqvist, P.-Å.; Veryazov, V.; Widmark, P.-O. New Relativistic ANO Basis Sets for Transition Metal Atoms. *J. Phys. Chem. A* **2005**, *109*, 6575–6579.

(54) Roos, B. O.; Lindh, R.; Malmqvist, P.-Å.; Veryazov, V.; Widmark, P.-O. Main Group Atoms and Dimers Studied with a New Relativistic ANO Basis Set. *J. Phys. Chem. A* **2004**, *108*, 2851–2858.

(55) Pierloot, K.; Vancoillie, S. Relative energy of the high-($^5T_{2g}$) and low-($^1A_{1g}$) spin states of $[Fe(H_2O)_6]^{2+}$, $[Fe(NH_3)_6]^{2+}$, and $[Fe(bpy)_3]^{2+}$: CASPT2 versus density functional theory. *J. Chem. Phys.* **2006**, *125*, 124303.

(56) Ghigo, G.; Roos, B. O.; Malmqvist, P.-Å. A modified definition of the zeroth order Hamiltonian in multiconfigurational perturbation theory (CASPT2). *Chem. Phys. Lett.* **2004**, *396*, 142–149.

(57) Douglas, N.; Kroll, N. M. Quantum electrodynamical corrections to the fine structure of helium. *Ann. Phys. (Leipzig)* **1974**, *82*, 89.

(58) Hess, B. Relativistic electronic-structure calculations employing a two-component no-pair formalism with external-field projection operators. *Phys. Rev. A* **1986**, *33*, 3742.

(59) Malmqvist, P.-Å.; Roos, B. O.; Schimmelpfennig, B. The restricted active space (RAS) state interaction approach with spin-orbit coupling. *Chem. Phys. Lett.* **2002**, *357*, 230–240.

(60) Roos, B. O.; Malmqvist, P.-Å. Relativistic quantum chemistry: the multiconfigurational approach. *Phys. Chem. Chem. Phys.* **2004**, *6*, 2919–2927.

(61) Etinski, M.; Tatchen, J.; Marian, C. M. Thermal and solvent effects on the triplet formation in cinnoline. *Phys. Chem. Chem. Phys.* **2014**, *16*, 4740–4751.

(62) Marian, C. M.; Nakagawa, S.; Rai-Constapel, V.; Karasulu, B.; Thiel, W. Photophysics of Flavin Derivatives Absorbing in the Blue-Green Region: Thioflavins As Potential Cofactors of Photoswitches. *J. Phys. Chem. B* **2014**, *118*, 1743–1753.

(63) Föller, J.; Kleinschmidt, M.; Marian, C. M. Phosphorescence or Thermally Activated Delayed Fluorescence? Intersystem Crossing and Radiative Rate Constants of a Three-Coordinate Copper(I) Complex Determined by Quantum-Chemical Methods. *Phys. Chem. Chem. Phys.* **2016**, *55*, 7508–7516.

(64) Rai-Constapel, V.; Marian, C. M. Solvent tunable photophysics of acridone: a quantum chemical perspective. *RSC Adv.* **2016**, *6*, 18530–18537.

(65) Li, Z.-F.; Zheng, Y.-Q. Synthesis and crystal structure of $[Fe(phen)_3]L{\cdot}2H_2L{\cdot}4H_2O$ (H_2L = fumaric acid). *J. Coord. Chem.* **2005**, *58*, 883–890.

(66) Braterman, P.; Song, J.-I.; Peacock, R. Electronic Absorption Spectra of the Iron(II) Complexes of 2,2'-Bipyridine, 2,2'-Bipyrimidine, 1,10-Phenanthroline, and 2,2':6',2"-Terpyridine and Their Reduction Products. *Inorg. Chem.* **1992**, *31*, 555–559.

(67) Sousa, C.; Domingo, A.; de Graaf, C. Effect of second-order spin-orbit coupling on the interaction between spin states in spin crossover systems. *Chem. Eur. J.* **2017**, *doi.org/10.1002/chem.201704854* .

Graph for Table of Contents